Published in *Soil Dynamics and Earthquake Engineering* 153 **2022** 107110

Seismic response of piles in layered soils: Performance of pseudostatic Winkler models against centrifuge data

Tott-Buswell, J.[a,1], Garala, T.K.[a,2], Prendergast L.J.[a,3], Madabhushi, S.P.G.[b,4], Rovithis, E.[c,5]

[a] Department of Civil Engineering,
Faculty of Engineering,
University of Nottingham,
Nottingham,
NG7 2RD,
United Kingdom

[b] Schofield Centre, Department of Engineering,
University of Cambridge,
Cambridge,
CB2 1PZ,
United Kingdom

[c] Institute of Engineering Seismology and Earthquake Engineering,
EPPO-ITSAK,
Eleones,
55535 Pylaia,
Thessaloniki,
Greece

[1]Corresponding Author

Email:

[1]jacques.tott-buswell@nottingham.ac.uk, [2]thejesh.garala@nottingham.ac.uk,
[3]luke.prendergast@nottingham.ac.uk, [4]mspg1@cam.ac.u k, [5]rovithis@itsak.gr

ORCID number:

[1]https://orcid.org/0000-0003-1621-329X, [2]https://orcid.org/0000-0001-7326-6596,
[3]https://orcid.org/0000-0003-3755-0391, [4]https://orcid.org/0000-0003-4031-8761,
[5]https://orcid.org/0000-0002-0331-5855

Abstract

In this study, the suitability of the pseudostatic approach for the seismic analysis of pile foundations in layered soils is explored by means of experimental data from centrifuge tests performed at 60*g*. A free-head single pile and a capped (1 × 3) pile group, embedded in a two-layered soil comprising a soft clay layer underlain by dense sand, are tested in the centrifuge under sinusoidal and earthquake excitations. For the pseudostatic analysis, a one-dimensional Winkler model is developed using hyperbolic *p*-*y* curves from design codes. The kinematic and inertial loads on the pile foundations are derived using the experimentally measured free-field soil displacements and accelerations, respectively. Different approaches of modifying the *p*-*y* relationship to account for soil layering are compared. The importance of considering peak spectral acceleration in lieu of peak ground acceleration at the soil surface to compute the inertial force for the pseudostatic analysis is highlighted. Pile group effects are investigated by considering *p*-multipliers from literature to account for pile-soil-pile interaction. Results reveal that: (i) for low-intensity seismic motions, the pseudostatic approach with inertial pile-head loading stemming from peak ground acceleration (PGA) at soil surface led to a reasonable agreement of the maximum bending moment with experimental data for both single pile and pile group, (ii) for high-intensity base excitations, the use of the peak spectral acceleration, instead of PGA, at soil surface with suitable damping considerations to derive the inertial load in the pseudostatic model provided a maximum bending moment prediction that was acceptable for the single pile but conservative for the piles in the group compared to the centrifuge records.

Keywords: Centrifuge; earthquake; layered soil; pile foundations; pseudostatic analysis

1 Introduction

Conventional pile design involves estimating the axial load capacity and satisfying the serviceability criteria in terms of allowable settlements and durability under static loads. In addition to axial loads, pile foundations are subjected to lateral dynamic loads during an earthquake due to: (i) the oscillation of the superstructure, which induces inertial loads at the pile head, and (ii) the ground deformation during the passage of seismic waves, which induce kinematic loads on pile foundations. Traditionally, kinematic loads are neglected in pile foundation seismic design as they are insignificant in comparison with inertial loads. However, the significance of kinematic loads has been highlighted by various post-earthquake reconnaissance reports [e.g., 1,2] and thus, several revised seismic codes recommend the consideration of kinematic loads in the seismic design of pile foundations under certain conditions (e.g., [3]). Nevertheless, there are no specific methodologies for the seismic design of pile foundations in design codes, resulting in various design approaches being followed by practitioners. These design approaches can range from very simplistic methods to complex computer analyses [4].

Despite recent developments in two- and three-dimensional dynamic finite element models including advanced soil constitutive behaviour, one-dimensional finite element or finite difference-based Winkler models are still widely employed for seismic soil-pile-structure interaction analysis due to their simplicity. In a Winkler (subgrade reaction) analysis, the pile is modelled as a series of linear elastic beams supported on discrete springs, the stiffness of which is characterized by a non-linear stiffness law reflecting soil-pile interaction [5–8]. The *p-y* method is a widely used approach for monotonic analysis that employs a non-linear relationship between the soil resistance, *p*, mobilised against the pile and the lateral displacement of the pile, *y*. Time domain dynamic analyses are computationally expensive and hence pseudostatic approaches using Winkler models are widely employed by practitioners. In dynamic analyses, the variation in response of the pile foundation with time-varying earthquake characteristics (intensity and frequency of excitation) is evaluated. However, in pseudostatic approaches, the maximum response (bending moment and shear force) of a pile foundation during an earthquake is estimated using a static inertial force with magnitude equal to the mass of the system times the acceleration of the excitation. A typical pseudostatic analysis for seismic loading involves two steps: (i) performing a seismic ground response analysis to obtain the maximum free-field soil displacement profile along the pile's length, and (ii) imposing a static force (peak inertial load) at the pile head and non-zero boundary conditions along the embedded pile informed by discretising the maximum free-field soil displacements (kinematic load). Abghari and Chai [9] presented the first pseudostatic analysis approach for piles in non-liquefying soils, by considering the inertial force acting at the pile head as the product of the cap-mass times a spectral acceleration as recommended by Dowrick [10]. To this end, an approximation is necessary to compute the associated natural period by considering the lateral pile-head stiffness [11]. By comparing the results of pseudostatic analysis with dynamic finite element analysis, the above authors concluded that 25% of the peak inertial force should be combined with the peak kinematic displacement for computing the peak pile deflection. Similarly, for computing the peak pile bending response, 50% of peak inertial force should be combined with peak kinematic displacement. Later, Tabesh and Poulos [11] contradicted this finding and recommended that imposing the total inertial force at the pile head can result in good agreement between the pseudostatic approach and dynamic analysis. Castelli and Maugeri [12] considered both kinematic and inertial loads and highlighted the suitability of pseudostatic approaches for the seismic analysis of single piles and pile groups.

In this study, the performance of pseudostatic approaches for the seismic analysis of pile foundations in layered soils is evaluated by comparison with centrifuge data. Centrifuge experiments were performed on a single pile and 1 × 3 row pile group embedded in a two-layered soil at 60g (g = gravitational acceleration) under sinusoidal and earthquake excitations. The soil profile consists of soft clay underlain by dense sand. Each centrifuge experiment was carried out in two flights, with acrylic Perspex and brass used as pile cap material in the first and second flight, respectively, to evaluate the individual contribution of kinematic and inertial loads on the pile foundations. Winkler analyses incorporating standard design-code recommended p-y relationships for laterally loaded piles were performed by considering both kinematic and inertial loads. The effect of soil layering on p-y relationships, magnitude of pseudostatic pile head (inertial) load, and pile group effects are discussed in detail.

2 Centrifuge tests description

Centrifuge experiments were conducted at 60g using the Turner beam centrifuge [13] facilities at the Schofield Centre, University of Cambridge, UK. In this series of experiments, the soil models were prepared with a dense, poorly graded, fraction-B Leighton Buzzard (LB) sand underlying soft speswhite kaolin clay to maintain significant stiffness contrast between the soil layers. The properties of fraction-B LB sand and speswhite kaolin clay can be found in Garala et al. [14]. For model pile foundations, a single pile and a 1 × 3 row pile group were fabricated using an aluminium (Alloy 6061 T6) circular tube of outer diameter (d) 11.1 mm and thickness (t) 0.9 mm. A centre-to-centre spacing of 3d is adopted between piles in the pile group. The bottom of the tubular piles is closed with an aluminium plug to restrict the entry of soil into the piles during pile installation. Further, the single pile and end piles of the pile group were strain gauged to measure the bending moments during earthquakes. Figure 1 shows the schematic view of the pile foundations used in the study along with the location of strain gauges. The centrifuge models were prepared from bottom to top, first by pouring the sand at the required relative density using an automatic sand pourer [15], followed by saturating the sand layer with de-aired water and then filling the model container with kaolin slurry for consolidation [16]. An air hammer device, a small actuator that can act as a source to induce waves within the soil model [17], was placed at the bottom of the model on a 10-15 mm thick sand layer during sand pouring. The detailed model preparation procedure and equivalent prototype characteristics of a single pile can be found in Garala [16] and Garala and Madabhushi [18]. The unit weight of the saturated clay and the sand is 16.2 kN/m^3 and 20.4 kN/m^3, respectively. Figure 2 shows the sectional view of the model along with the location of various instruments used in the model. Piezoelectric accelerometers were used to measure the accelerations in the soil model at different depths, micro-electro-mechanical-system accelerometers were used on top of pile caps to measure the accelerations, and pore pressure transducers were used to measure the pore-water pressures at different depths. Further, each centrifuge experiment was carried out in two flights, with acrylic plexiglass used as pile caps in flight-01 (hereafter referred to as K flight) and pile caps made from brass in flight-02 (hereafter referred to as K+I flight), to examine the effects of kinematic and combined kinematic and inertial loads, respectively. The mass of the plexiglass caps for single pile and the pile group are 11 grams and 24 grams at model scale, respectively. These masses are less than half the self-weight of the pile foundations (each model pile weighs 24 grams without strain gauges) and are negligible compared with the axial load-carrying capacity of the single pile (0.57 kg at model scale). Hence, the pile accelerations and bending moments measured during K flight can be considered as the effect of kinematic loads alone. In K+I flight, the brass caps will induce a static vertical force of 167.75 N and 503.25 N at model scale (0.604 MN and 1.812 MN at prototype scale) for the single pile and the pile group, respectively; therefore, the vertical load acting per pile is the same for both the single pile and the pile groups.

A T-bar 40 mm wide and 4 mm in diameter was used to determine the undrained shear strength (c_u) of the clay layer. To measure the soil stiffness, the air hammer device was activated and the propagation of shear waves through the soil profile was measured using an array of piezo-electric accelerometers placed on above the air hammer device (see Fig. 2). Figures 3a and 3b show the c_u profile of the clay layer determined from the in-flight T-bar test and the small-strain shear modulus (G_0) of the soil layers determined from the air hammer device, respectively, before subjecting the model to base excitations. G_0 values determined from published expressions [19–21] are also shown in Fig. 3b. By considering an average G_0 of 23 MPa and 184 MPa for the clay and sand layers (at a depth of 4d-5d above and below the interface), respectively, a sharp stiffness contrast between the two soil layers is obtained, referring to a small-strain shear modulus ratio ($G_{0,sand}/G_{0,clay}$) equal to 8. Further, a quite large $G_{0,clay}/c_u$ ratio around 2300 was obtained for the clay layer. Figure 4 shows the acceleration time-histories of the base excitations (BE) considered in this study, including sinusoidal excitations of different driving frequencies and increasing intensity along with a scaled 1995 Kobe earthquake motion.

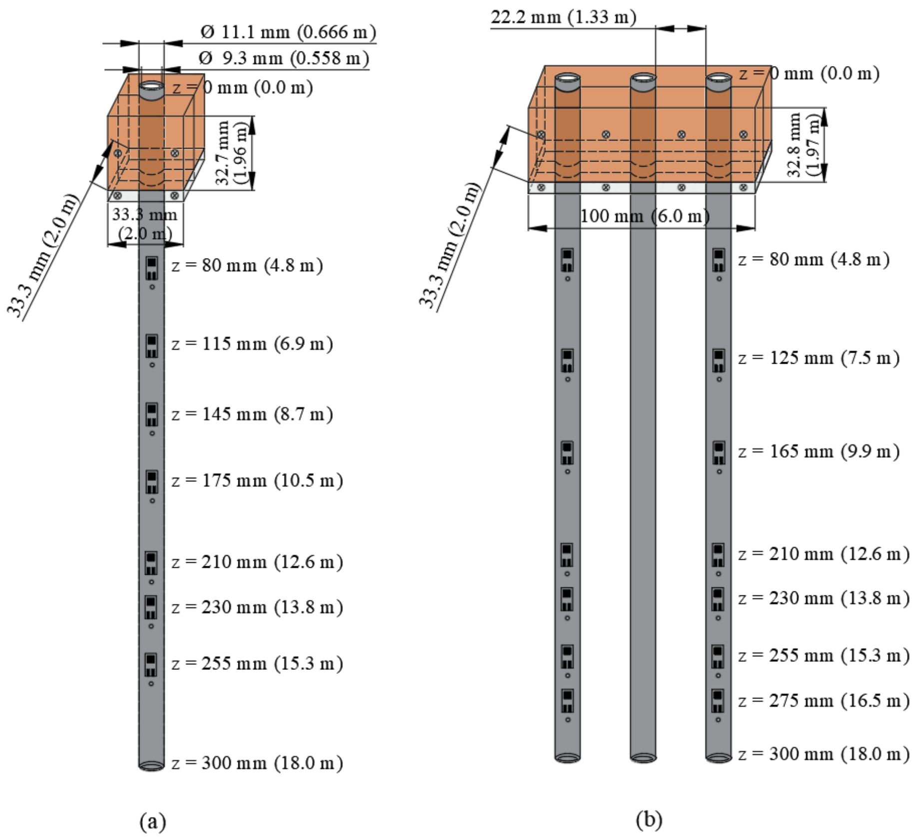

Figure 1. Schematic view of tested pile foundations: (a) single pile and (b) pile group (prototype dimensions in parentheses)

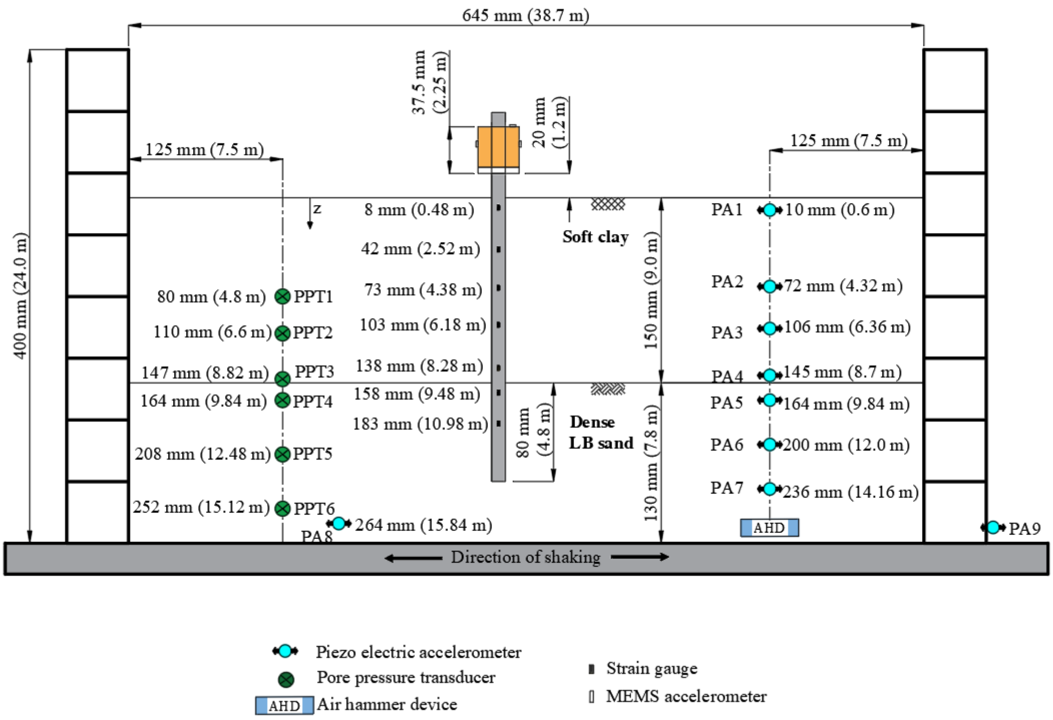

Figure 2. Sectional view of the centrifuge model with instruments and pile foundation (prototype dimensions in parentheses)

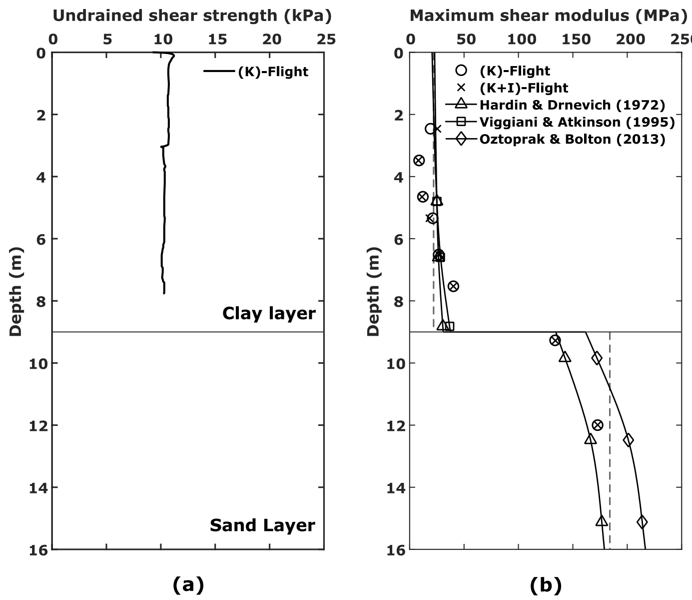

Figure 3. (a) Undrained shear strength of clay layer from T-bar test and (b) Maximum shear modulus of soil layers from air-hammer tests

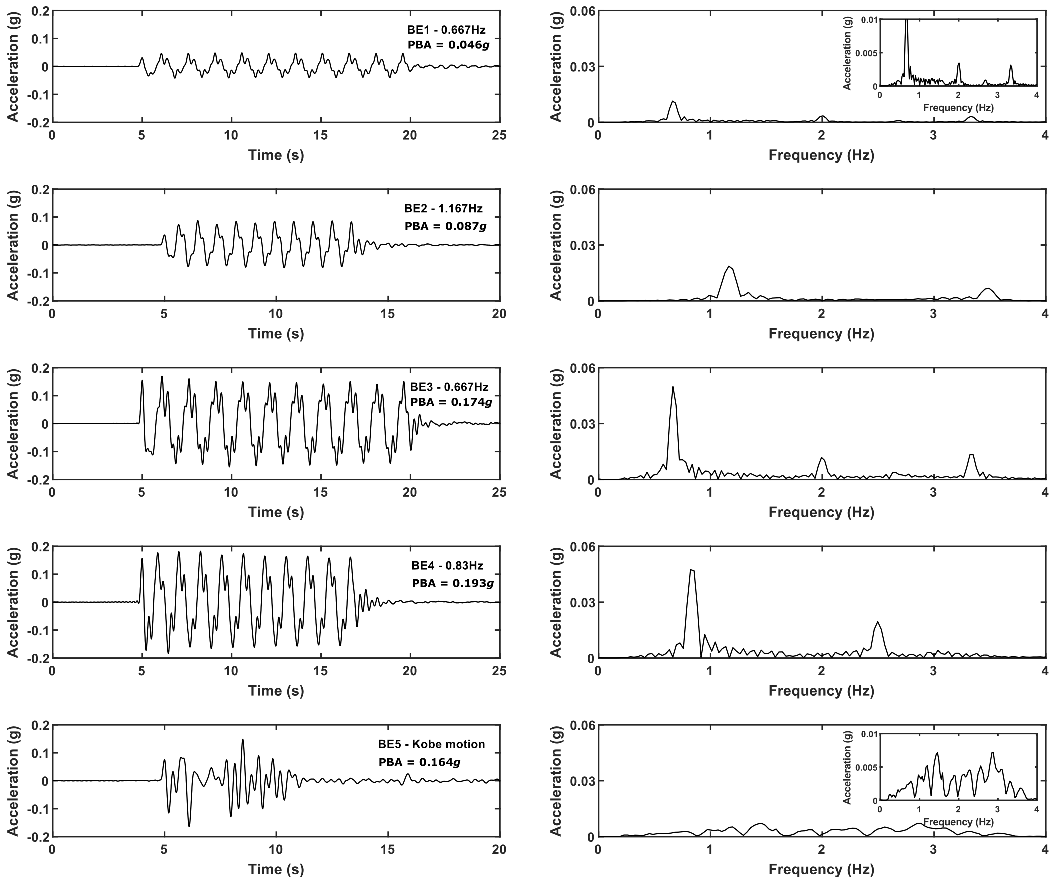

Figure 4. Acceleration time-histories and corresponding fast Fourier transforms of base excitations BE1 to BE5

3 Pseudostatic Modelling Procedure

The pseudostatic model employed herein is presented in Fig. 5 following Tabesh and Poulos [11]. The Beam on Non-linear Winkler Foundation (BNWF) model consists of a series of linear-elastic Euler-Bernoulli beam elements supported on non-linear *p-y* spring elements at discrete points to represent the pile and soil, respectively. The ordinary differential equation of a beam on a Winkler foundation is given by:

$$E_p I_p \frac{d^4 y_p}{dz^4} - p(y_{el}) - F_I = 0 \tag{1}$$

where E_pI_p is the flexural stiffness of the pile, y_p is the pile displacement, p is the soil pressure function, y_{el} is the spring element's displacement, referring to the relative displacement between the free-field soil displacement y_s and the pile deflection y_p (i.e. $y_{el} = y_p - y_s$), and F_I is the inertial load.

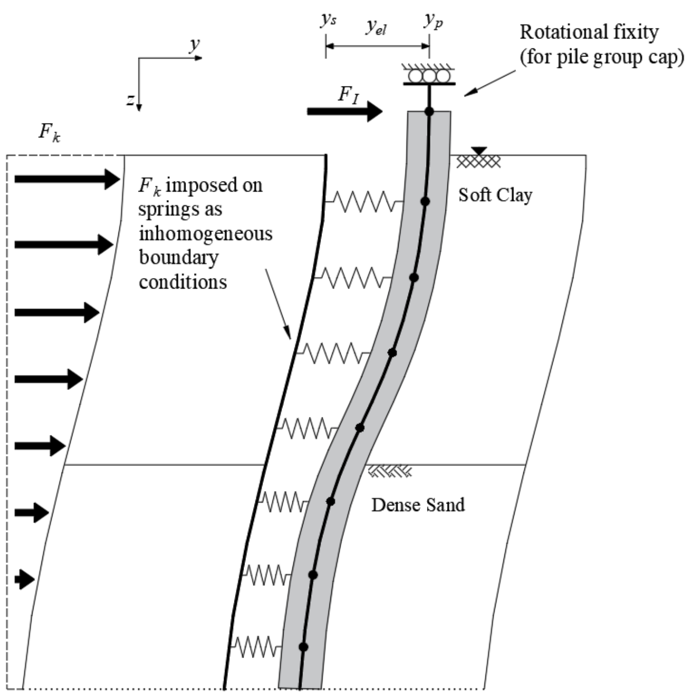

Figure 5. p-y_{el} model illustration for pseudostatic modelling of a capped pile in multi-layered soils

The continuous form of the equilibrium equation can be solved using the direct stiffness method by discretising the physical system appropriately. The pseudostatic model considers both kinematic and inertial loadings in the following manner:

1. Kinematic loading F_k induced from the free field soil lateral displacement y_s is modelled through imposing y_s as inhomogeneous boundary conditions on the spring elements as informed through the maximum soil displacements recorded in the centrifuge tests for a given base

excitation. It should be noted that the maximum soil displacements at each depth may have occurred at different times. Values are linearly interpolated where necessary for nodal displacement values within the discretised Winkler model.

2. Inertial loading $F_I = M_{cap}(\ddot{y}_s)$ due to the pile cap mass is modelled as a single point load applied at the pile head , where M_{cap} is the mass of the pile cap and $\ddot{y}_s$ can be either the peak ground acceleration or the peak spectral acceleration recorded in the centrifuge at soil surface for a given base excitation.

A rotational fixity is assumed at the pile head location for the pile group to simulate pile cap boundary conditions and for the single pile case the pile head is free to rotate. The lateral soil pressure p is computed based on y_{el}. The function used to describe the p-y_{el} element depends on the layer in which the corresponding spring resides. For the present study, American Petroleum Institute (API) [22] recommended p-y relationships were used for the clay and sand layer, where $y = y_{el}$. It should be noted that the p-y curves in [22] were developed for laterally loaded pile foundations using full-scale monotonic and cyclic pile-head lateral load field tests on long piles in different soil conditions. For these reasons, the p-y functions may not be suitable for pile response analysis under dynamic loading. However, as there are no dynamic p-y_{el} curves recommended in the codes, cyclic p-y relationships are used in this study as defined by API [22] for simplicity.

3.1 API p-y model for soft clays

The p-y_{el} curves for the clay layer are constructed as a function of the ultimate lateral resistance ($p_{u,1}$) and the lateral pile displacement at one-half the ultimate lateral resistance (y_c), calculated as $y_c = 2.5\varepsilon_c d$, where d is the diameter of the pile [23]. In the absence of experimental stress-strain curves, a representative value for ε_c can be adopted in terms of c_u [24]. For an average c_u of 11 kPa (Fig. 3(a)), Sullivan et al. [24] recommended $\varepsilon_c = 0.02$. For soft clays with constant unit weight and shear strength in the upper zone of the pile, a transition depth (z_r) must be defined to describe the depth at which spring ultimate capacities shift from a passive wedge-type failure mechanism at shallow depths to a block-type failure mechanism at greater depths:

$$z_r = \frac{6c_u d}{\gamma_1' d + J c_u} \tag{2}$$

where γ'_1 is the unit weight of the clay and J is an experimentally derived dimensionless constant taken as 0.5 for soft clay [23]. The ultimate capacity of the clay spring element is therefore defined as $p_{u,1} = p_{us,1}$ for $z_1 \leq z_r$ and $p_{u,1} = p_{ud,1}$ for $z_1 > z_r$, where:

$$p_{us,1} = \left(3 + \frac{\gamma_1'}{c_u} z_1 + \frac{J}{D} z_1\right) c_u d \tag{3}$$

$$p_{ud,1} = 9 c_u d \tag{4}$$

Note that Eq. (2) is obtained by equating Eq. (3) and (4) and setting $z_1 = z_r$, where z_1 is the depth of the upper layer spring element. The corresponding API clay function for soil resistance in the first layer (p_1) within the region exhibiting a shallow failure mechanism is described through the piecewise expression:

$$p_1 = \begin{cases} \frac{p_{us,1}}{2}\left(\frac{y_{el}}{y_c}\right)^{1/3} & \text{for } y_{el}/y_c \leq 3 \\ 0.72p_{us,1} & \text{for } y_{el}/y_c > 3 \end{cases} \tag{5}$$

For deep failure mechanisms, the API clay spring element is defined by Eq. (6).

$$p_1 = \begin{cases} \frac{p_{ud,1}}{2}\left(\frac{y_{el}}{y_c}\right)^{1/3} & \text{for } y_{el}/y_c \leq 3 \\ 0.72p_{ud,1}\left[1-\left(1-\frac{z_1}{z_r}\right)\left(\frac{y_{el}/y_c-3}{12}\right)\right] & \text{for } 3 < y_{el}/y_c \leq 15 \\ 0.72p_{ud,1}\left(\frac{z_1}{z_r}\right) & \text{for for } y_{el}/y_c > 15 \end{cases} \tag{6}$$

To prevent an initial infinite tangent stiffness with the current API clay *p-y* definition, the initial stiffness of the clay spring elements is defined by $K_1 = 0.5p_{u,1}L_1/y_c$, where L_1 is the tributary beam element length for the clay layer [25] and $p_{u,1}$ is the appropriate ultimate soil resistance value defined by either Eq. (3) and (4).

3.2 API p-y model for sands

The method proposed by O'Neill and Murchinson [26] for sands is defined by the hyperbolic tangent relationship described in Eq. (7).

$$p_2 = Ap_{u,2}\tanh\left(\frac{kz_2}{Ap_{u,2}}y_{el}\right) \tag{7}$$

where p_2 is the soil reaction of the sand layer, A is an adjustment factor and is taken as 0.9 for cyclic loading, k is the depth-independent coefficient of subgrade reaction, and z_2 is the depth of soil elements in the sand layer. $p_{u,2}$ is the ultimate lateral resistance of the sand element and is described using the following expressions:

$$p_{u,2} = \min(p_{us,2}, p_{ud,2}) \tag{8}$$

$$p_{us,2} = (C_1z_2 + C_2d)\sigma'_{v,2} \tag{9}$$

$$p_{ud,2} = C_3d\sigma'_{v,2} \tag{10}$$

where C_1, C_2 and C_3 are dimensionless constants which are functions of the sand's angle of internal friction ϕ', and $\sigma'_{v,2}$ is the vertical effective stress in the sand (i.e. $\sigma'_{v,2} = \gamma'_2 z_2$). Details on computing C_1, C_2, C_3 and k can be found in [22]. It is important to note that the transition depth of failure type z_r for sands is not explicitly defined and the ultimate lateral resistance is therefore taken as the minimum of the two failure definitions as shown in Eq. (8). The initial stiffness of the sand spring elements is defined as the first derivative of Eq. (7) with respect to y_{el} at zero deflection.

3.3 Soil layering effects

Design standards for laterally loaded piles do not explicitly advise any specific *p-y* curves to account for layered soils or any suggestions to modify the above *p-y* curves of homogeneous soils for use with layered soils [22]. Therefore, in the presence of layered soils, underlying soil spring element functions must be modified accordingly to account for the change in vertical stresses imposed by upper soil layers. For soft clay underlain by dense sand, it is expected that the sand's strength would be less than what API's hyperbolic definition suggests, as the lighter clay imposes a lower overburden pressure at the soil interface depth than what would be expected in a fully homogeneous dense sand deposit. Therefore, the p-y_{el} functions describing the sand's lateral resistance to pile motion must be modified.

In the present study, the upper layer of soft clay is modelled by using the API functions for clay under cyclic loading [23] without any modifications. Two methods are used to modify the sand's p-y_{el} curves. In the first method (Method A), the depth at which API functions for sand are computed is modified by calculating an equivalent height (h_2) above the interface depth H_1 that would provide a lateral capacity equivalent to the original overlying soil layer, as recommended by Georgiadis [27]. Using $z_2 = H_1 - h_2$ as the effective groundline depth for API sand functions in Eqs. (7) to (10) ensures that the lateral capacity above $z=H_1$ is fully considered when deriving the spring functions below the interface depth. This method is illustrated in Fig. 6 and demonstrates the lateral capacities of the pile-soil interaction which are defined by the areas within the respective p_u functions in Eq. (3), (4), (9) and (10). Equating the two hatched areas defined by the failure criteria of sand and clay above the interface depth H_1, the appropriate effective depth h_2 can be calculated.

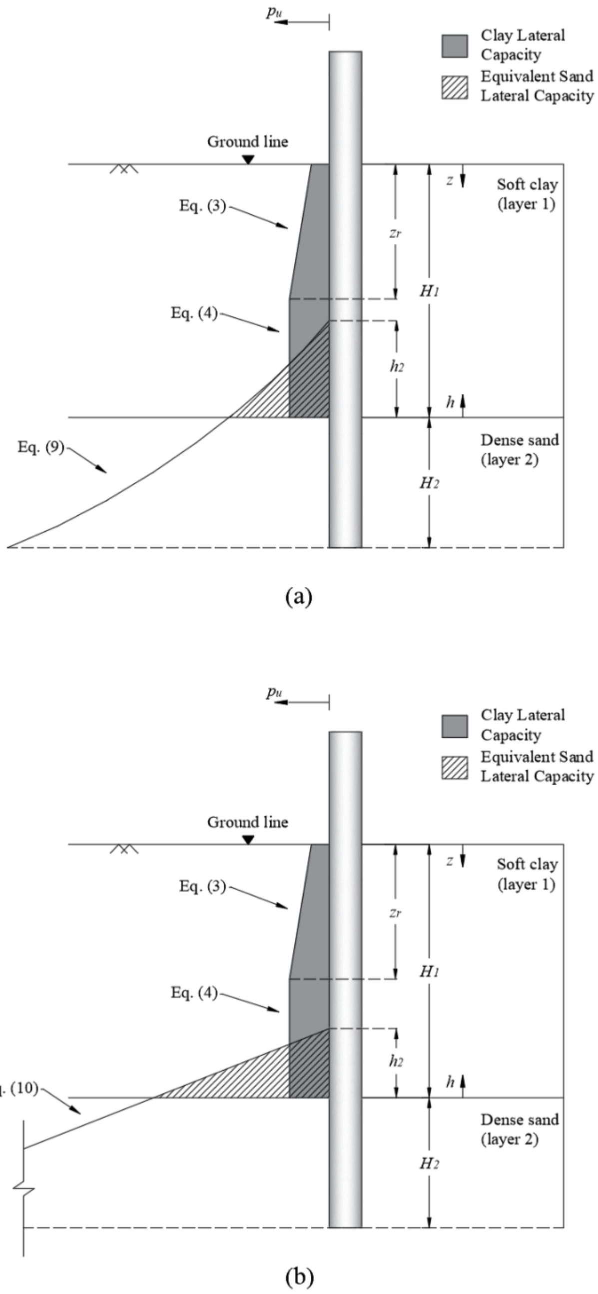

Figure 6. Failure criteria for (a) shallow sand failure, and (b) deep sand failure

Denoting the hatched areas in Fig. 6 as F_1, the lateral capacity of the soft clay can be expressed analytically as follows:

$$F_1 = \int_0^{z_r} p_{us,1} dz + \int_{z_r}^{H_1} p_{ud,1} dz = \int_0^{h_2} p_{u,2} dh \tag{11}$$

where h_2 is the effective depth of sand to be solved for. Note that the clay layer below z_r has constant ultimate lateral resistance proportional to the undrained shear strength, as defined by Eq. (4). It is also important to note that h_2 varies depending on the failure function for the ultimate resistance of the sand, as shown in figure 6(a) and 6(b). As it was not specified in Georgiadis [27] which failure definition should be considered for the given stratum, both shallow and deep failure definitions are evaluated for the underlying dense sand layer. Solving Eq. (11) gives $h_2 = 3.07$ m for the shallow sand failure criterion from Eq. (9), and $h_2 = 1.40$ m from the deep failure criterion Eq. (10).

In method B, the layering effect is considered by imposing the upper clay layer as an overburden stress on the lower sand layer through a modification in Eq. (9) to (10) such that the sand's ultimate resistance increases (i.e. $\sigma'_{v,2} = \gamma'_2 z_2 + \gamma'_1 H_1$) and the effective depth z_2 of the lower layer springs is now measured from the interface depth. This method will result in a lower bound value for the ultimate resistance of the sand layer, as suggested by Georgiadis [27].

The model is solved under both kinematic and inertial loading through non-homogenous boundary conditions and a nodal point load, respectively. The global secant stiffness matrix is computed based on Euler-Bernoulli beam theory and the secant stiffness k_{el} of each spring's p-y_{el} curve $k_{el} = p/y_{el}$, where the displacement and moment profiles of the pile are computed by iteration. The pseudostatic model is developed in MATLAB's coding environment. 60 clay spring elements and 30 sand spring elements are evenly spaced across H_1 and H_2 respectively. A sensitivity study showed that additional springs had negligible influence on the global response of the pile.

4 Pile group effects on *p-y* curves

The term 'group effects' refers to the influence piles exert on the behaviour of nearby piles. The p-y_{el} relationships discussed above are applicable only for single piles. Pile groups under lateral loads will generally exhibit less lateral capacity than the sum of the lateral capacities of the individual piles. This is due to the so-called "shadowing" effect, referring to the interference of the failure planes of the piles in trailing rows with the failure planes of the piles in front of them. For this reason, the piles in the trailing rows exhibit less lateral resistance [28]. Similar to the behaviour of pile groups under axial loads, the group efficiency of laterally loaded pile groups increases with the ratio of pile spacing (s) over pile diameter (d). Rollins et al. [28] recommends that pile group effects under lateral loading may be considered negligible for a pile spacing of the order of $6d \sim 8d$. For lower values of piles' spacing, the "shadowing" effect is usually treated by employing an efficiency factor, commonly referred to as p-multipliers within the p-y curve concept. This relates the force driving the pile group to the force required to displace a single pile an equal distance [29]. The p-y_{el} curves for the piles in a group are modified using p-multipliers, which reduce both the stiffness and the ultimate lateral capacity of the piles in a group with respect to the single pile case.

Table 1 provides a summary of pile group p-multipliers proposed by various researchers based on physical model and field tests in clays and sands for pile groups subjected to monotonic and cyclic lateral loads at the pile head. A more comprehensive list of p-multipliers can be found in [30].

Table 1. Group interaction factors under lateral loads from previous studies.

Study	Soil type	Pile spacing	Group efficiency factor	*p*-multipliers by row			
				Row 1	Row 2	Row 3	Row 4
Brown et al. [31]	Clay	3*d*	0.68–0.80	0.70	0.60	0.50	-
Rollins et al. [32]	Clay	2.83*d*	0.59-0.80	0.60	0.38	0.43	-
Snyder [33]	Clay	3.92*d*	0.85-0.90	1.00	0.81	0.59	0.71
Rollins et al. [34]	Clay	3.3*d*	0.45-0.67	0.90	0.61	0.45	0.45
	Clay	4.4*d*	0.75-1.00	0.90	0.80	0.69	0.73
	Clay	5.65*d*	0.87-0.90	0.94	0.88	0.77	-
Brown et al. [29]	Sand	3*d*	0.63-0.70	0.80	0.40	0.30	-
Ruesta and Townsend [35]	Sand	3*d*	0.60-0.91	0.80	0.70	0.30	0.30
Rollins et al. [28]	Sand	3.3*d*	0.72-0.935	0.80	0.40	0.40	-

As Table 1 shows, *p*-multipliers for the leading-row piles are significantly higher than those for the trailing-row piles. It is important to ensure that the head fixity condition of a single pile and pile groups is similar before implementing any efficiency factors, as the pattern of flexural deformation will be fundamentally different between the two. Literature related to *p*-multipliers under time-varying dynamic loading conditions is limited (e.g., [36]).

5 Acceleration response of soil strata and pile foundations

Figure 7a shows the peak acceleration measured at different depths of soil strata during each base excitation (BE1–BE5) in K and K+I centrifuge flights. The peak soil displacement profile, determined by double integration of the recorded soil accelerations, is shown in Fig. 7b. The amplification of motion as shear waves propagate from the dense sand layer to the surface of the soft clay layer can be clearly seen in Figs. 7a and 7b. More details about the dynamic response of tested soil-strata and the comparison of response from centrifuge soil-strata with one-dimensional seismic ground response analysis can be found in Garala and Madabhushi [37]. Figure 8 shows the acceleration response at the soil surface and the pile-cap as recorded during the two flights of centrifuge testing (see Fig. 2 for accelerometer locations). The soil-strata responded similarly in both flights, except for BE4 excitation. As expected, the pile accelerations are different in K flight and K+I flight, with the pile acceleration amplitude being larger in K+I flight compared to K flight in most cases due to the presence of inertial loads in K+I flight.

However, for the single pile, the pile accelerations in K+I flight are smaller than in K flight at some loading cycles during BE2, BE4 and BE5 excitations. This is due to the phase difference between the kinematic and inertial loads. For the same tested pile foundations, Garala and Madabhushi [18] has shown that there is a significant phase difference between the kinematic and inertial loads for the single pile during BE2, BE4 and BE5 excitations and hence the pile accelerations in K+I flight are smaller than those in K flight. For all other cases, the kinematic and inertial loads act together or with smaller phase difference, leading to larger pile accelerations in K+I flight compared to K flight. The significant phase difference between the kinematic and inertial loads also leads to lower pile bending moments as the piles are vibrating with smaller acceleration amplitudes. More details about the phase difference between the kinematic and inertial loads and its influence on pile accelerations and bending moments can be found in Garala and Madabhushi [18].

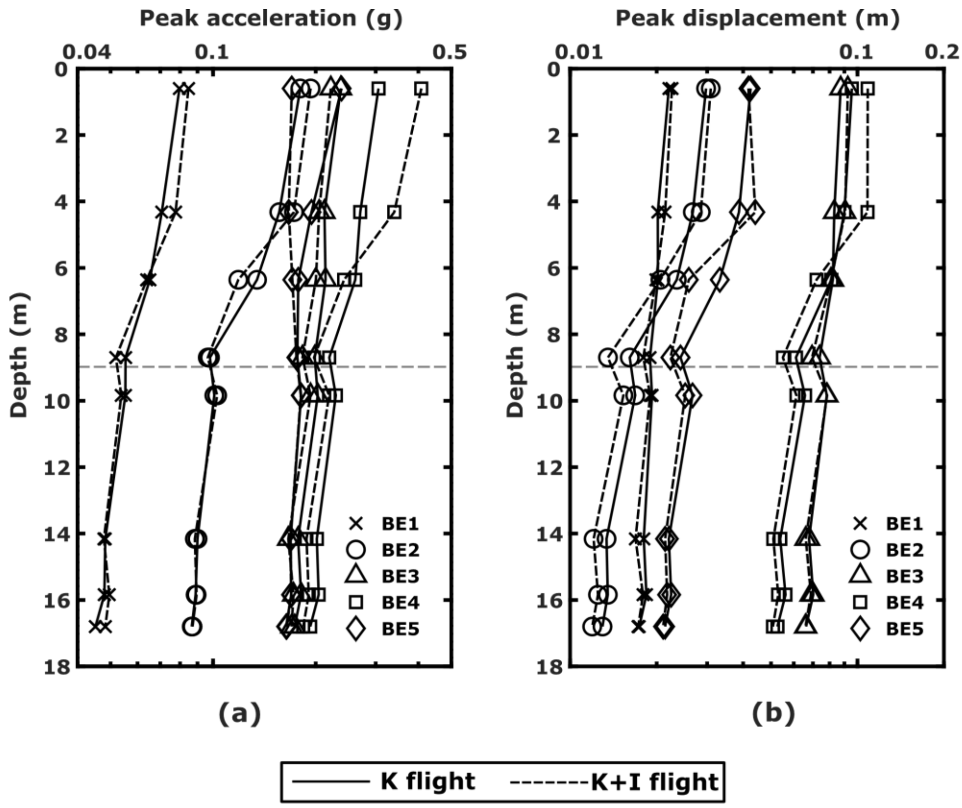

Figure 7. (a) peak accelerations and (b) peak displacements in the soil strata at different depths

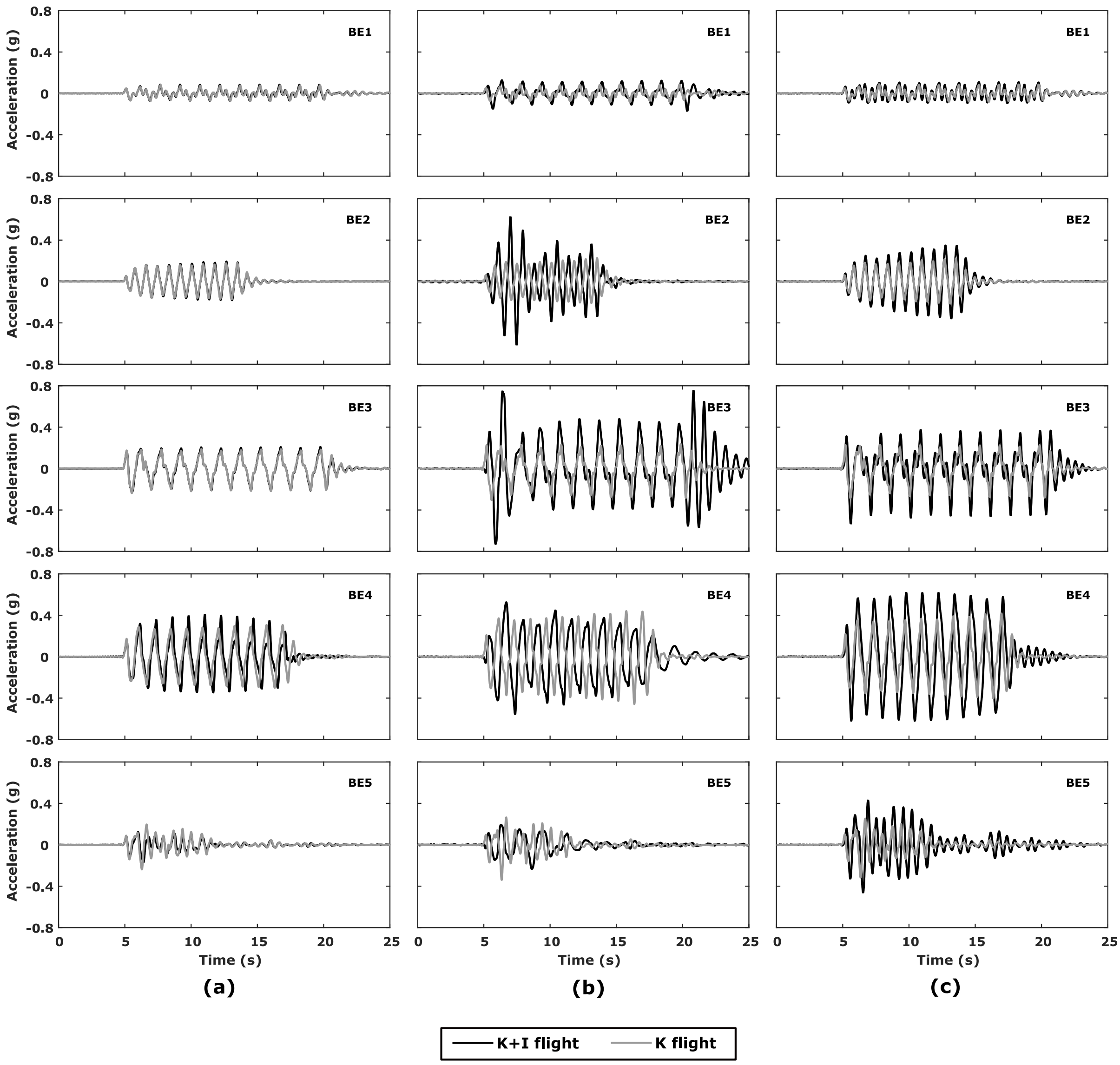

Figure 8. Acceleration time histories of (a) soil surface, (b) single pile, and (c) pile group during different excitations in K and K+I flights

6 Kinematic pile bending moments

In centrifuge experiments, strain gauges distributed along the pile continuously measure the bending moments during different base excitations for both the single and pile group (end piles only, see Fig. 1) for both flights. The measured bending moments in the K flight are considered as the kinematic pile bending moments (M_k). Bending at the pile tip is assumed to be zero for both the single pile and end piles in the group for both flights and only the response measured by one end pile in a group is used for the numerical comparison.

M_k from the pseudostatic model is determined using Method A and Method B by considering no inertial load at the pile cap location. Figures 9 and 10 show the comparison of peak M_k from centrifuge data and the pseudostatic model for the single pile and pile group, respectively. As Fig. 9 shows, the results from the numerical model always underestimate the peak M_k of the single pile. Compared to the peak M_k of the single pile determined from centrifuge experiments, the numerical study based on Method A (with shallow failure criteria) under-predicts the peak M_k by a minimum of 32% (during BE1) and maximum of 82% (during BE4). Similarly, Method A (with deep failure criteria) underestimates the peak M_k by a minimum of 32% (during BE1) and maximum of 79% (during BE5). The peak M_k of the single pile from the numerical study based on Method B underestimates the peak M_k by a minimum of 50% (during BE1) and maximum of 87% (during BE5) in comparison to centrifuge data. It can also be derived from Fig. 9 that the percentage difference between peak M_k from the pseudostatic model based on Method A (with shallow failure criteria) and Method B is a minimum of 21% (during BE3) and maximum of 40% (during BE2) for the single pile. Similarly, the percentage difference between Method A's shallow and deep failure criteria is a minimum of 10% (during BE2) and maximum of 27% (during BE3) for the single pile. For the pile group, the pseudostatic method under-predicts the peak M_k by a minimum of 5% (during BE1) and maximum of 80% (during BE3) using both Method A and Method B in comparison to centrifuge data (see Fig. 10). The maximum percentage difference between peak M_k from the numerical study based on Method A (deep failure criteria) and Method B is 46% (during BE1) for the pile group. This indicates that the earthquake intensity and pile cap rotational constraint critically govern the accuracy of the pseudostatic results. For the pile group with pile cap rotational constraint, the difference between Method A and Method B is negligible for larger intensity earthquakes. While computing M_k for the pile group from the numerical method, no *p*-multipliers were used for pile groups as group effects are usually neglected for the kinematic loads [2,38]. Therefore, it is clear from Figs. 9 and 10 that the pseudostatic method highly underestimated the kinematic pile bending moments for both the single pile and pile group and the difference increases with the intensity of the excitation. This is to be expected as the adopted code-based *p-y* curves are not developed for seismic kinematic loads.

For evaluating pile bending under seismic kinematic loads, several simplified procedures and analytical solutions have been proposed in the literature. Margason and Halloway [39] assumed that the pile foundation follows the surrounding soil motion during earthquakes and evaluated the pile bending response based on the free-field soil curvatures using the finite-difference method. Despite its simplicity, the Margason and Halloway [39] method showed satisfactory performance in predicting the pile head moment in homogeneous or two-layer soils with the soil interface at deeper depths [40,41]. Nevertheless, the Margason and Halloway [39] method is not useful for a layered soil profile with sharp stiffness contrast between the layers. In this case, Dobry and O'Rourke [42], Nikolaou et al. [43], Mylonakis [44], Nikolaou et al. [2] and Di Laora et al. [45], Di Laora and Rovithis [46],among others, have proposed closed-form solutions for evaluating the peak M_k based on beam on Winkler foundation or finite-element analyses. Garala et al. [14] evaluated the accuracy of these analytical and numerical solutions by comparing with experimental centrifuge data. The study of Garala et al. [14] revealed that only a few methods in the literature can reasonably estimate the peak M_k. The importance of considering soil nonlinearity effects and accurate shear strains at the interface of soil layers for a reliable assessment of the kinematic pile bending moment from the methods in existing literature is also highlighted in Garala et al. [14].

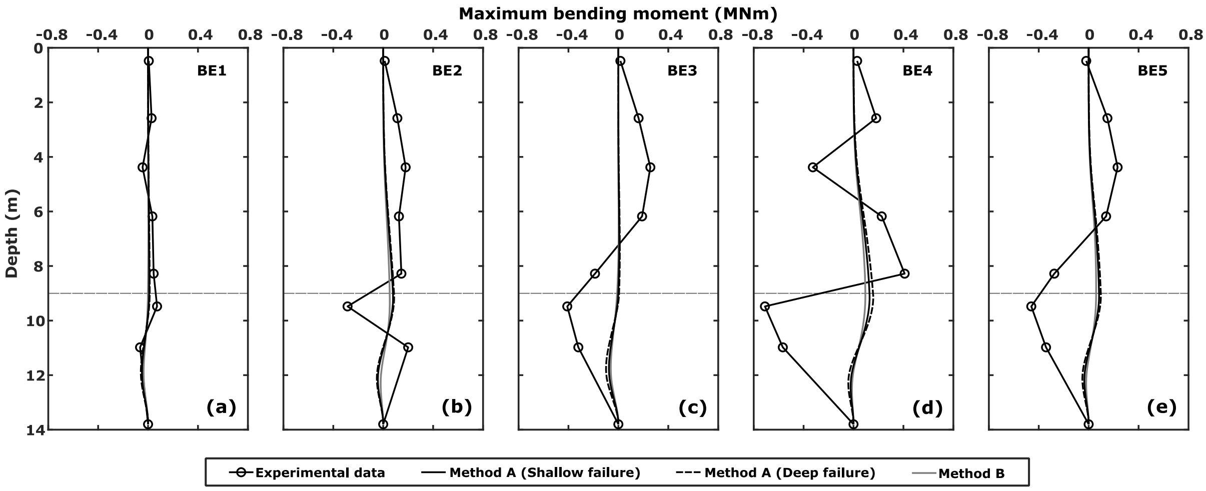

Figure 9. Comparison of kinematic pile bending moments obtained from centrifuge experiment and numerical study for single pile

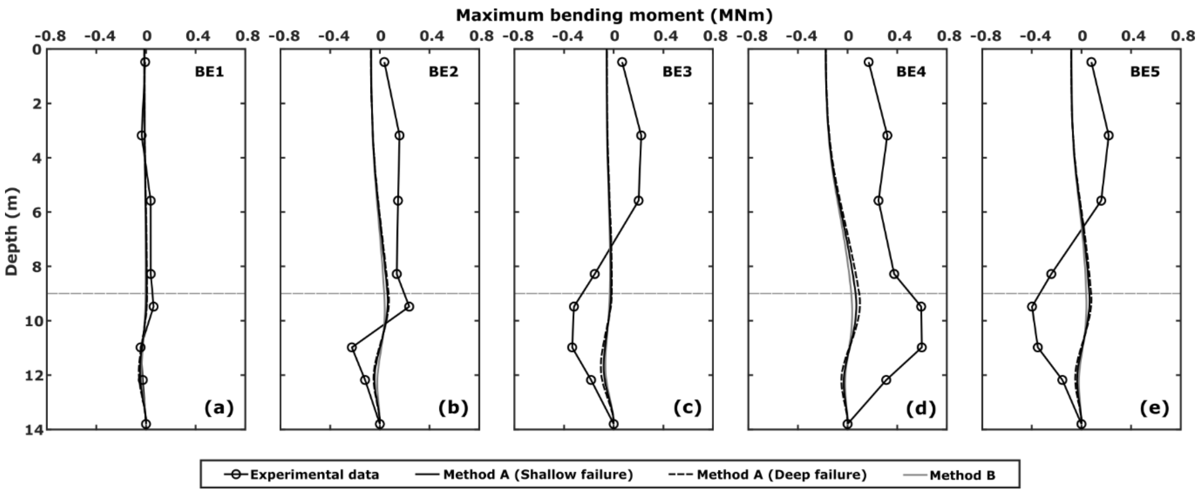

Figure 10. Comparison of kinematic pile bending moments obtained from centrifuge experiment and numerical study for pile group

7 Combined kinematic and inertial effects

For computing the pseudostatic inertial force at the pile head, either maximum free field soil acceleration or peak spectral acceleration can be considered along with the mass of the pile cap. In the case of liquefiable soils, Abghari and Chai [9] found that considering the spectral acceleration for the inertial force resulted in the overestimation of pile response. On the other hand, Tabesh and Poulos [11] recommended to consider either peak ground acceleration or peak spectral acceleration depending on the relevance between the dominant period of the pile-cap-soil system and the frequency content of the surface motion. According to Tabesh and Poulos [11], the former may be approximated by the expression $T=2\pi\sqrt{(M_{cap}/K_x)}$, where K_x is the lateral head stiffness of the pile. However, the above expression involving a crude approximation of reducing the mass of the supporting structure to a pile-cap mass should be used with caution as any eccentricity of the superstructure mass may have an important effect on the response. In this regard, the above authors suggested that for the case of relatively small pile-cap masses, the natural frequency of pile-cap-soil system may not be within the dominant frequencies of the ground surface motion, denoting negligible inertial effects. For such cases, the free-field soil motion governs pile behaviour, and the pseudostatic analysis can be performed by considering the peak ground acceleration at soil surface. For larger pile-cap masses that can have dominant frequencies close to the dominant frequencies of surface motion, inertial effects may be significant. Under these circumstances, Tabesh and Poulos [11] recommended to consider the peak spectral acceleration rather than the maximum soil surface acceleration as considering peak spectral acceleration can yield a conservative result. The recommendations of Tabesh and Poulos [11] suggest that the ground natural frequency and that of the pile cap-structure govern whether kinematic or inertial loads dominate. The studies of Adachi et al. [47] and Tokimatsu et al. [48] also recommend that whether kinematic or inertial loads dominate is a function of the relevance between the natural frequencies of the soil and the pile-supported superstructure. However, recently, Garala and Madabhushi [18] concluded that whether kinematic or inertial loads dominate pile response is independent of the natural frequency of the soil and the phase relationship between the kinematic and inertial loads follows the conventional force-displacement phase variation for a viscously damped simple oscillator excited by a harmonic force. In this study, to keep the analysis simple, the kinematic and inertial loads are assumed to act together on the pile foundations, indicating in-phase loading conditions. Further, due to the uncertainty in choosing the peak soil surface acceleration or the peak spectral acceleration for computing the inertial force in pseudostatic analysis, both are considered in this study and the quantitative difference between the two is evaluated by comparing the results with centrifuge data.

First, the maximum soil surface acceleration from centrifuge experiments was considered to compute the pseudostatic inertial force. Figure 11 shows the comparison of centrifuge data and the pseudostatic model for the single pile. The numerical results based on Method A (both shallow and deep failure criteria) and Method B for combined kinematic and inertial loads can be seen along with the pure inertial loads. Table 2 shows the under-prediction (negative values) or over-prediction (positive values) of peak bending moment by the pseudostatic analysis in comparison with the peak bending moment from centrifuge data. As Fig. 11 and Table 2 indicate, the pseudostatic analysis based on peak ground acceleration under-estimates the peak bending moment during all earthquakes. The difference between the experimental values and the numerical study is relatively lower in those excitations where the pile bending moment is smaller due to the significant phase difference between the kinematic and inertial loads (BE4 and BE5 excitations), see Garala and Madabhushi [18] for more details about the influence of phase difference between kinematic and inertial loads on pile bending moments. Further, the maximum percentage difference between Method A (shallow criteria) and Method B in the pseudostatic models is only 5.5% (during BE5) for the single pile. Similarly, the maximum percentage difference between shallow and deep failure criteria in Method A is only 2.1% (during BE5) for the single pile. This suggests that there is no significant difference in peak bending moment predicted by considering either the top-layer as overburden or an equivalent depth for the bottom layer, following Georgiadis [27] procedure with shallow or deep failure criteria to account for soil-layering effects. It should be noted that this might be valid only for the case of soils with significant stiffness contrast between the layers. Also, it can be observed from Table 2 that there is no significant difference between pseudostatic results from Method A/Method B and pure inertial loads. This is due to the inability of the current numerical model in capturing the actual pile kinematic response, as discussed above.

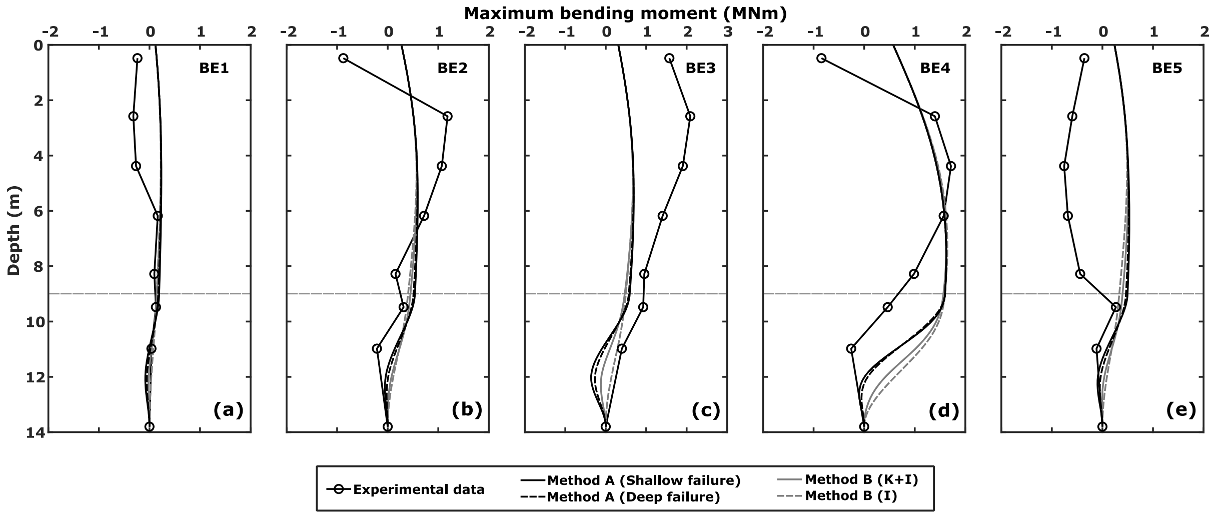

Figure 11. Comparison of pile bending moments obtained from centrifuge experiment and numerical study for single pile

For the case of the pile group, the reduction of stiffness and ultimate capacity is accounted for through p-multipliers, as discussed earlier. Table 1 shows the p-multipliers proposed by various researchers for pile groups under non-dynamic lateral loads in sands and clays. As a single row pile group is tested in the centrifuge experiments, an average conservative value of the p-multiplier (p) of 0.7 is considered for both the clay and sand layers from Table 1, given that p-multipliers depend primarily on piles' spacing rather than soil layering [12]. Figs. 12 and 13 show the comparison of peak pile bending moments computed from pseudostatic analysis and centrifuge data for p = 1 (i.e., neglecting group effects) and p = 0.7, respectively. Table 3 shows the under-prediction (negative values) or over-prediction (positive values) in peak bending moment by the pseudostatic analysis in comparison to the peak bending moment from centrifuge data. It is clear from Figs. 12 and 13 and Table 3 that the pseudostatic analysis can better predict the peak bending moment in the piles of a pile group compared to a single pile. Further, considering the group effects through *p*-multipliers will increase the magnitude of overprediction for certain excitations (BE1 to BE3) and reduces the difference between actual (or centrifuge) and model predicted moments for large intensity excitations (BE4 and BE5), as shown in Table 3. As can be seen from experimental data in Fig. 12, the piles in a pile group will have significant bending moments both at the interface of layered soils and at shallower depths close to the pile cap. Though the pseudostatic model captures well the peak bending moment at the shallower depths, it highly underestimates the peak bending moment at the interface of layered soils, especially during medium to large intensity base excitations. This is again due to the inability of the pseudostatic model in capturing the true kinematic pile response. Further support on the above is also provided by the negligible difference between the peak bending moment values determined by considering both kinematic and inertial loads and by inertial loads alone (see Table 3). Further, similar to the case of the single pile, the maximum percentage difference between peak bending values from Method A (deep failure criteria) and Method B in numerical analysis is only 1.3% (BE1). Nevertheless, Method A predicted the peak bending moments at the interface of layered soils slightly better than Method B though none of the methods can capture the true kinematic pile response (see Figs. 12 and 13). This indicates that soil layering effects can be considered either by equivalent depth approach or just by considering the top layer as overburden on the bottom layer for the case of soil strata with significant stiffness contrast for the fixed-head pile group. Nevertheless, this approach will not predict the peak bending moments at the interface of layered soils to an acceptable level.

Table 2. Quantitative comparison of peak bending moment from pseudostatic analysis with the peak bending moment from centrifuge experiments for single pile (K+I flight)

Base excitation	Method A (Shallow failure)	Method A (Deep failure)	Method B (K+I loading)	Method B (I loading)
BE1	-26.2%	-27.3%	-29%	-29.4%
BE2	-49.8%	-50.3%	-51.2%	-51.8%
BE3	-66.8%	-67%	-67.8%	-67.8%
BE4	-5.4%	-5.4%	-5.4%	-4.2%
BE5	-29.7%	-31.1%	-33.4%	-35.5%

('- ve' sign indicates the under-prediction in comparison to experimental value and vice-versa)

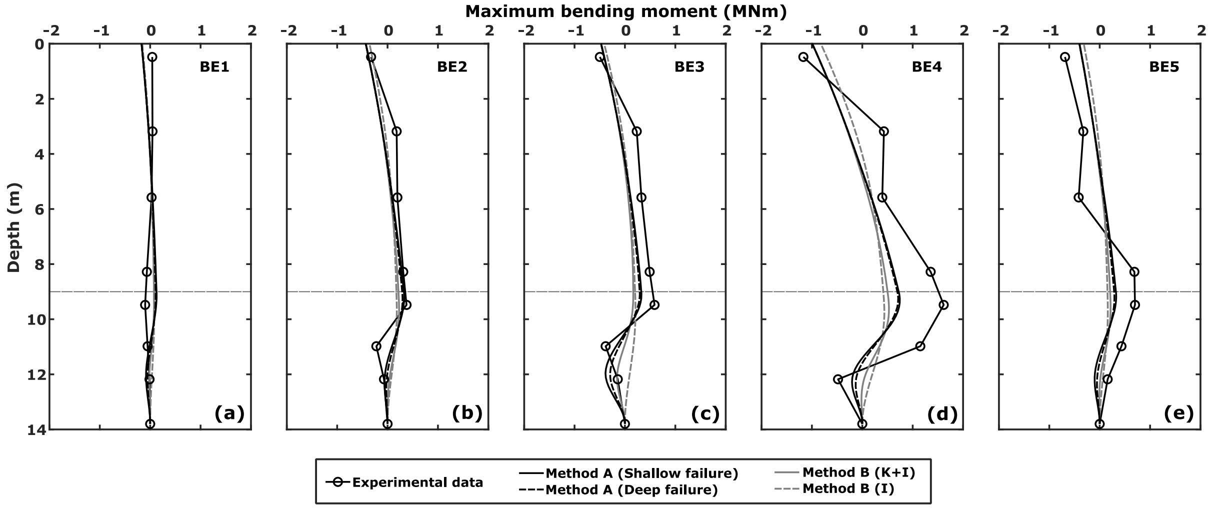

Figure 12. Comparison of pile bending moments obtained from centrifuge experiment and numerical study for a pile in pile group with *p*-multiplier (*p*) = 1

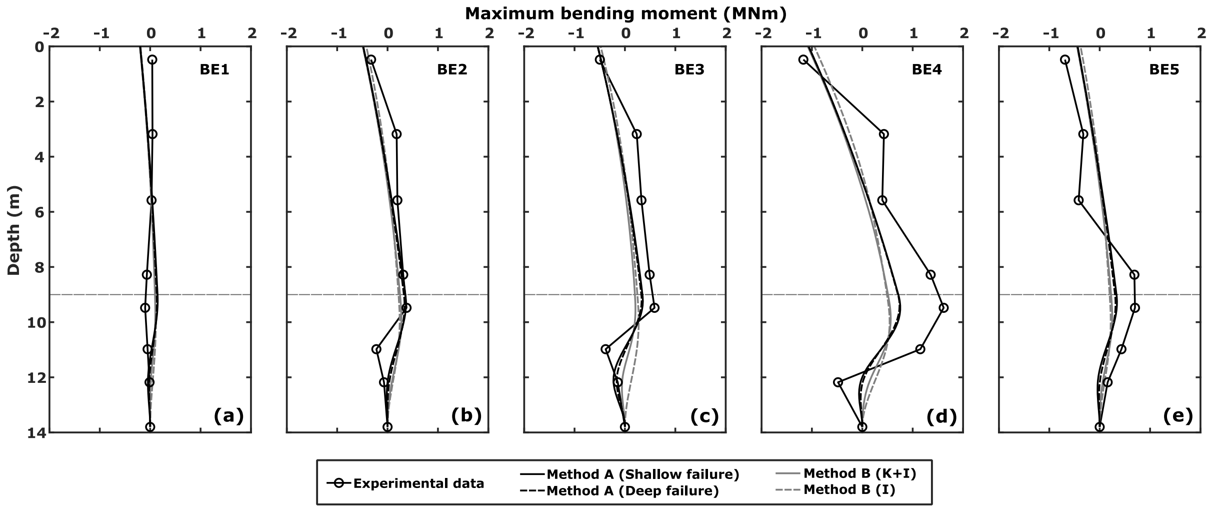

Figure 13. Comparison of pile bending moments obtained from centrifuge experiment and numerical study for a pile in pile group with *p*-multiplier (*p*) = 0.7

Table 3. Quantitative comparison of peak bending moment from pseudostatic analysis with the peak bending moment from centrifuge experiments for pile group (K+I flight)

Base excitation	*p*-multiplier = 1			*p*-multiplier = 0.7		
	Method A (Shallow failure)	Method B (K+I loading)	Method B (I loading)	Method A (Shallow failure)	Method B (K+I loading)	Method B (I loading)
BE1	132.7%	130.6%	118.5%	158.9%	164.2%	153.8%
BE2	52.1%	50.7%	32.4%	65%	67.6%	49.1%
BE3	8.3%	7.3%	-2.7%	19.6%	18.9%	9.3%
BE4	-20.2%	-20.4%	-30.8%	-15.7%	-14.6%	-22.7%

BE5	-24.9%	-25.6%	-37.4%	-20%	-18.5%	-28.2%

('- ve' sign indicates the under-prediction in comparison to experimental value and vice-versa)

Figs. 11 to 13 suggest that considering the peak ground acceleration at soil surface in computing the pseudostatic inertial force might result in satisfactory results only for the pile group, but not for the free-headed single pile. Therefore, to further investigate the suitability of the pseudostatic approach, peak spectral accelerations are considered for computing the pseudostatic inertial forces for the base excitations under consideration. Figure 14 shows the spectral accelerations computed for 10% and 20% damping from the recorded soil surface accelerations. Pile response from pseudostatic analysis is computed by considering the peak spectral acceleration magnitude for each base excitation from Fig. 14. It is important to note that for low damping ratios (≤10%), some inertial loads F_1 were too large for numerical compliance, and therefore are not shown in the study.

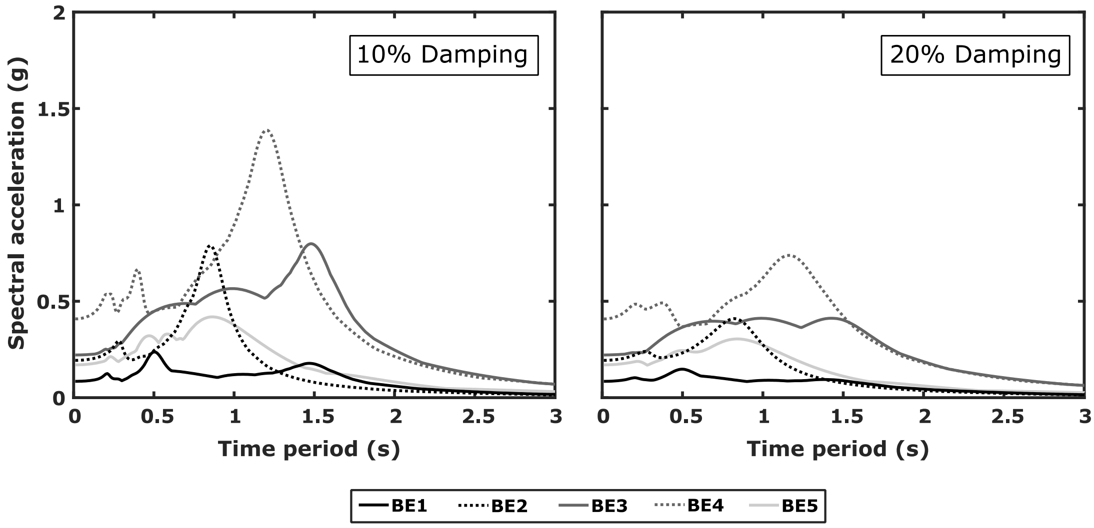

Figure 14. Spectral accelerations determined from soil surface accelerations for 10% and 20% damping ratios

Figures 15 and 16 show the comparison of peak bending moments of the single pile from experiments and the pseudostatic model by considering inertial forces computed from peak spectral accelerations at 10% and 20% damping, respectively. Method A with deep failure criteria and pure inertial loads are not considered while plotting Figs. 15 and 16 due to the smaller difference between deep failure and shallow failure criteria from Method A and between kinematic and inertial loads and inertial loads alone from Method B, as discussed earlier. Table 4 shows the under-prediction (negative values) or over-prediction (positive values) of peak bending moment by the numerical analysis in comparison to the peak bending moment obtained from centrifuge experiments. The pseudostatic model failed for BE4 excitation with 10% damping due to larger inertial forces and hence no values were reported for this case in Fig. 15 and Table 4. As Fig. 15 and Table 4 shows, the bending moments determined from numerical analysis highly overestimate the bending moment value from centrifuge experiments for the single pile at 10% damping. However, the pseudostatic model resulted in an acceptable bending moment value at 20%

damping for the single pile, as shown in Fig. 16 and Table 4. As the clay is very soft, 20% damping seems quite acceptable. Nevertheless, the location of peak bending moment is not the same from centrifuge experiments and numerical analysis for the single pile as shown in Figs. 15 and 16. Therefore, considering inertial forces from peak spectral acceleration magnitudes with appropriate damping in the pseudostatic analysis might result in obtaining a peak bending moment value close to that of the actual value for a free-headed single pile. Nevertheless, the location of peak bending moment may not be accurate from the pseudostatic analysis for piles in layered soils.

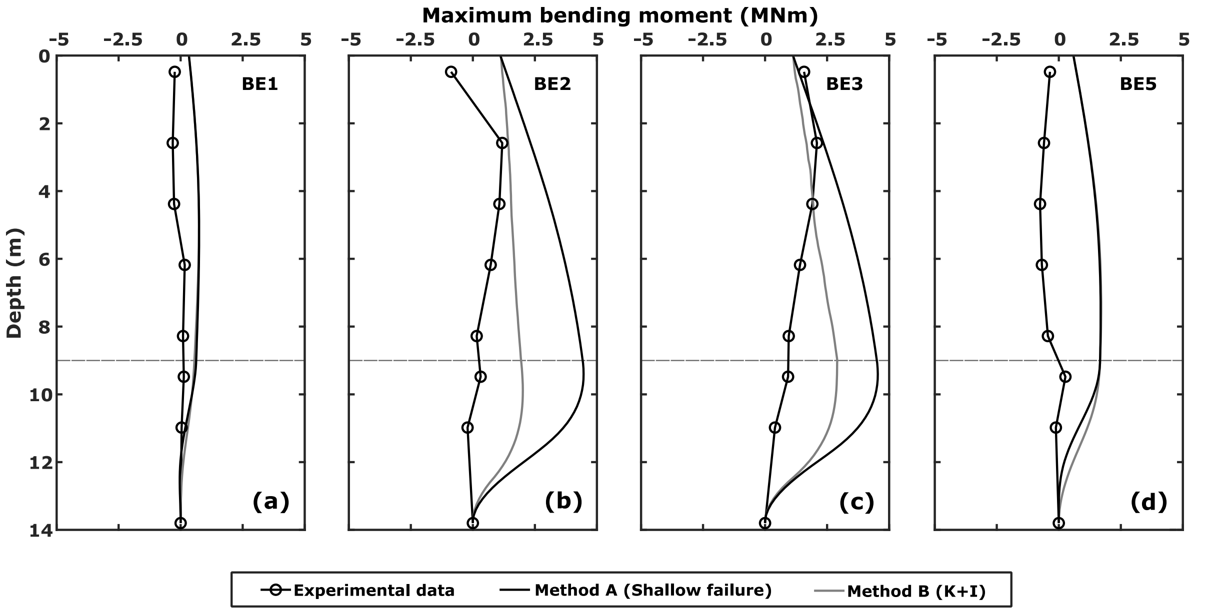

Figure 15. Comparison of pile bending moments obtained from centrifuge experiment and numerical analysis for single pile from spectral accelerations with 10% damping

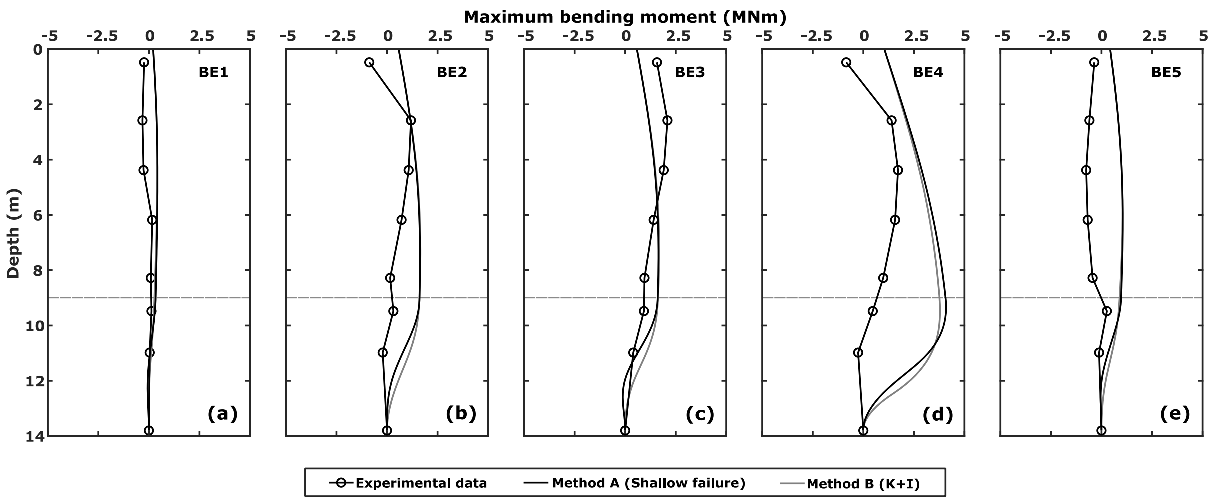

Figure 16. Comparison of pile bending moments obtained from centrifuge experiment and numerical analysis for single pile from spectral accelerations with 20% damping

For the case of the pile group, Figs. 12 and 13 and Table 3 show that considering the peak ground acceleration for computing the pseudostatic inertial force will result in an acceptable peak pile bending response for certain excitations (BE1 to BE3). Obviously, considering the spectral acceleration even at higher damping of 20% will result in a highly conservative peak bending value for the pile group, as shown in Figure 17 and Table 5. However, considering the spectral acceleration for the pile group improved the efficiency of the pseudostatic model in capturing the pile bending response at the interface of layered soils. As Fig. 17 shows, there is a relatively smaller difference in peak bending moment value between the numerical study and experimental data at the interface of layered soils compared to the corresponding difference shown in Figures 12 and 13. For smaller intensity excitations, the numerical analysis over-predicted the bending moment at the interface of layered soils, for example by 150% during BE1 by Method B with $p = 0.7$. However, at larger intensity excitations, the maximum difference between the experimental value and numerical analysis is -51% during BE5 (Method B with $p = 1$).

Table 4. Quantitative comparison of peak bending moment from pseudostatic analysis using spectral acceleration with the peak bending moment from centrifuge experiments for single pile

Base excitation	10% Damping		20% Damping	
	Method A (Shallow failure)	Method B (K+I loading)	Method A (Shallow failure)	Method B (K+I loading)
BE1	133.3%	130.4%	32.6%	30.1%
BE2	277.1%	70.2%	37.8%	39.4%
BE3	117.4%	39.2%	-21.3%	-19.8%
BE4	-	-	138.4%	120.7%
BE5	122.8%	125.6%	38.8%	37.3%

(‘- ve’ sign indicates the under-prediction in comparison to experimental value and vice-versa)

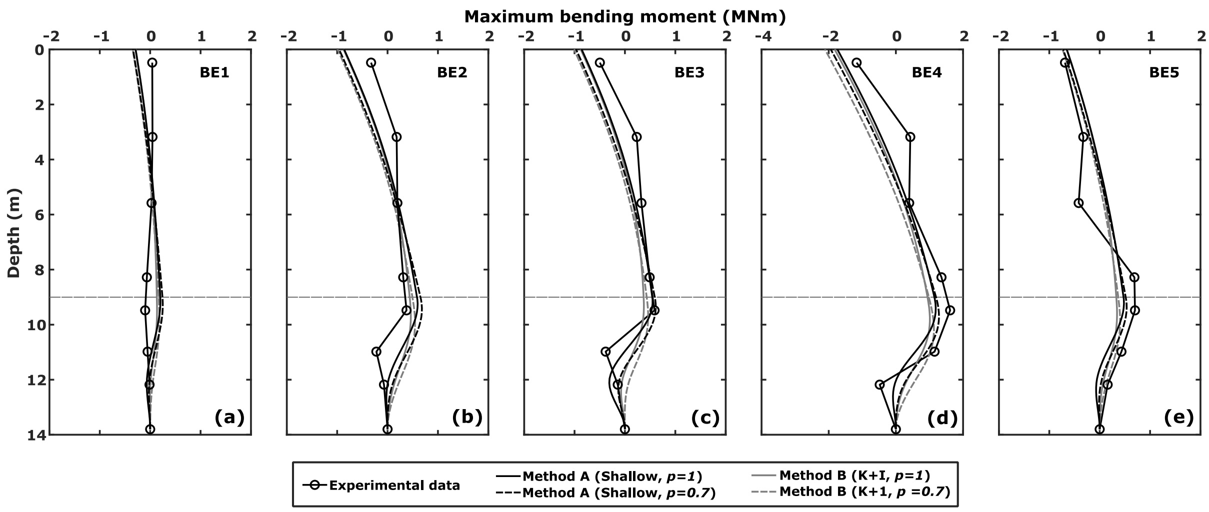

Figure 17. Comparison of pile bending moments obtained from centrifuge experiment and numerical analysis for pile group from spectral accelerations with 20% damping

Table 5. Quantitative comparison of peak bending moment from pseudostatic analysis using spectral acceleration with the peak bending moment from centrifuge experiments for pile group

Base excitation	*p*-multiplier = 1		*p*-multiplier = 0.7	
	Method A (Shallow failure)	Method B (K+I loading)	Method A (Shallow failure)	Method B (K+I loading)
BE1	297.1%	293.9%	346.7%	353.9%
BE2	207.2%	210.2%	233.8%	2.42%
BE3	97%	100.2%	116%	122.8%
BE4	40.9%	46%	53.1%	63.8%
BE5	24.8%	24.2%	34.7%	36.4%

('- ve' sign indicates the under-prediction in comparison to experimental value and vice-versa)

8 Conclusions

The efficacy of pseudostatic approaches in the seismic analysis of pile foundations in layered soils is discussed in this study by comparing the performance of pseudostatic models with centrifuge records. The latter were obtained from centrifuge tests on a single pile and a 1 × 3 row pile group at 60*g* to evaluate the pile bending moments due to kinematic and inertial loads. The soil profile consists of a soft clay layer underlain by dense sand. A finite element model for pseudostatic analysis was developed that consists of a series of linear-elastic Euler-Bernoulli beam elements and non-linear *p-y* spring elements at discretised points taking the form of a BNWF model. In this study, API [22] recommended *p-y* relationships for the laterally (monotonic or cyclic) loaded piles were used for the clay and sand layer. The pseudostatic model considers both kinematic and inertial loads by considering peak free-field soil displacements and maximum inertial loads at the pile head, respectively. The effect of soil layering on p-y_{el} relationships was accounted for by considering the concept of equivalent depths proposed by Georgiadis [27] and by considering the top-layer as an overburden on the bottom layer. Pile-group effects in soil-pile interaction were accounted for by reducing the stiffness and ultimate capacity of the pile group using the concept of *p*-multipliers. The following are the observations from this study:

- As expected, the adopted BNWF model implementing the API (2014) *p-y* relationships was not able to capture the kinematic pile bending at the interface of the examined layered soil profile, as the above *p-y* curves refer to piles in homogeneous soils subjected to monotonic or cyclic loads. In this regard, the numerical model under-predicted the kinematic pile bending moments in the range of 32% to 87% depending on the intensity of base excitations.
- The peak bending moments computed for combined kinematic and inertial loads from pseudostatic analysis using inertial forces computed from peak ground acceleration at soil surface may under-predict the value for a free-headed single pile by 4.2% to 67.8% depending on the procedure followed to incorporate the soil layering effects. However, for the pile group,

the proposed pseudostatic model can over-predict the peak bending (when pile group effects are disregarded by setting the *p*-multiplier at 1) in the range of 7.3% to 132.7% for small to medium intensity excitations and underestimates the peak bending by 2.7% to 37.4% for larger intensity excitations. The performance of the pseudostatic model for the pile group can be improved by considering appropriate average *p*-multipliers to account for pile group effects.

- Irrespective of single pile or pile group, it was observed that the pseudostatic model failed at capturing the actual pile bending moments at the interface of layered soils when the inertial force was derived from peak ground acceleration at the soil surface.
- On the contrary, the performance of the pseudostatic model for the single pile was improved when the peak spectral acceleration was considered to derive the inertial force acting at the pile-head. Using this approach, the pseudostatic model mostly over-predicted the actual bending moments, and the percentage difference depended on the damping considered while computing the peak spectral accelerations from measured soil surface accelerations. This is valid even for the piles in a pile group.
- While incorporating the soil layering effects, a significant difference between Georgiadis [27] shallow and deep failure criteria was observed while computing the peak kinematic pile bending moments. However, in the presence of both kinematic and inertial loads, the maximum percentage difference between values computed from Georgiadis [27] shallow and deep failure criteria is only 2.1%. Similarly, the difference between Georgiadis [27] approach and the overburden approach is significant in the presence of kinematic loads alone, but negligible in the presence of both kinematic and inertial loads for most cases. This is true only while comparing the peak bending moment values.

Overall, during small intensity base excitations and for non-resonance conditions, the code recommended *p*-*y* curves results in an acceptable range of peak bending moment values in comparison to centrifuge data for a free-headed single pile and piles within a pile group by considering peak ground acceleration in pseudostatic methods. However, at large intensity excitations where the soil behaviour is highly non-linear, a reasonable estimation of pile bending moments can be made from pseudostatic methods by considering peak spectral accelerations while computing the pseudostatic inertial forces. Further, as discussed in this article, the soil layering effects on *p*-*y* curves can be accounted for either by implementing the Georgiadis [27] suggestions or by treating the top layer as an over-burden on bottom layer (for soil profiles similar to the one discussed in this article). Nevertheless, both theories account for the effect of overlying layers on the lower layers but not vice-versa. Relevant studies based on finite element simulations (e.g., [50]) have demonstrated that layering effects can act in two directions, namely that the *p*-*y* response of the upper layers can also be affected by the presence of lower layers. This aspect of soil layering effects is not considered in the equivalent depth approach proposed by Georgiadis [27] or where the top layer is treated as an overburden on the bottom layer. Furthermore, it should be mentioned that the seismic response of pile foundations is governed by lateral motions and axial stresses induced by rocking of the single pile, or group, on piles of a pile group. Lateral motion in only one direction is considered in this analysis, and a more realistic seismic pile behaviour can be captured by modelling both lateral motion and rocking together. Moreover, the model's modular framework can include alternative monotonic *p-y* functions to encapsulate soil-structure interaction, such as PISA [51] and CPT-based derivations [52–54], which may be more appropriate for pseudostatic analysis in layered soil deposits. However, only soil stiffness is considered in such models, and advanced analysis in the time domain can be performed by incorporating dashpots and hysteretic soil elements to capture the dynamic response of the soil-structure system more appropriately.

Acknowledgements

The first author wishes to acknowledge funding for their PhD under EP/R513283/1 EPSRC Standard Research Scholarship (DTP) at the Faculty of Engineering, University of Nottingham, UK.

References

[1] Mizuno H. Pile damage during earthquakes in Japan. ASCE Geotech Publ 1985:53–78.

[2] Nikolaou S, Mylonakis G, Gazetas G, Tazoh T. Kinematic pile bending during earthquakes: Analysis and field measurements. Geotechnique 2001;51:425–40. https://doi.org/10.1680/geot.2001.51.5.425.

[3] EC8. Design Provisions for Earthquake Resistance of Structures, Part 5: Foundations, Retaining Structures and Geotechnical Aspects. CEN Eur Comm Stand 2000;CEN/TC250.

[4] Poulos HG. Designing piles for seismic events. DFI Melb 2017:1–28.

[5] Winkler E. Die Lehre von Elastizitat und Festigkeit (on Elasticity and Fixity). Dominicus, Prague: 1867.

[6] Kampitsis AE, Sapountzakis EJ, Giannakos SK, Gerolymos NA. Seismic soil–pile–structure kinematic and inertial interaction—A new beam approach. Soil Dyn Earthq Eng 2013;55:211–24. https://doi.org/10.1016/J.SOILDYN.2013.09.023.

[7] Prendergast LJ, Gavin K. A comparison of initial stiffness formulations for small-strain soil–pile dynamic Winkler modelling. Soil Dyn Earthq Eng 2016;81:27–41. https://doi.org/10.1016/j.soildyn.2015.11.006.

[8] Rovithis E, Kirtas E, Pitilakis K. Experimental p-y loops for estimating seismic soil-pile interaction. Bull Earthq Eng 2009;7:719–36. https://doi.org/10.1007/s10518-009-9116-7.

[9] Abghari A, Chai J. Modeling of soil-pile-superstructure interaction for bridge foundations. Perform. Deep Found. under Seism. Load., 1995, p. 45–59.

[10] Dowrick DJ. Earthquake resistant design. A manual for engineers and architects. Publ Wiley Sons, Ltd 1977.

[11] Tabesh A, Poulos HG. Pseudostatic Approach for Seismic Analysis of Single Piles. J Geotech Geoenvironmental Eng 2001;127:757–65. https://doi.org/10.1061/(asce)1090-0241(2001)127:9(757).

[12] Castelli F, Maugeri M. Simplified approach for the seismic response of a pile foundation. J Geotech Geoenvironmental Eng 2009;135:1440–51. https://doi.org/10.1061/(ASCE)GT.1943-5606.0000107.

[13] Schofield AN. Cambridge Geotechnical Centrifuge Operations. Geotechnique 1980;30:227–68. https://doi.org/10.1680/geot.1980.30.3.227.

[14] Garala TK, Madabhushi SPG, Di Laora R. Experimental investigation of kinematic pile bending in layered soils using dynamic centrifuge modelling. Géotechnique 2020:1–16. https://doi.org/10.1680/jgeot.19.p.185.

[15] Madabhushi SPG, Haigh SK, Houghton NE. A new automated sand pourer for model preparation at University of Cambridge. Proc. Int. Conf. Phys. Model. Geotech., 2006, p. 217–222.

[16] Garala TK. Seismic Response of Pile Foundations in Soft Clays and Layered Soils. (Doctoral Thesis) University of Cambridge, 2020. https://doi.org/doi.org/10.17863/CAM.52405.

[17] Ghosh B, Madabhushi S. An efficient tool for measuring shear wave velocity in the centrifuge. Int. Conf. Phys. Model. Geotech., St. Johns, Newfoundland: Balkema; 2002, p. 119–24.

[18] Garala TK, Madabhushi SPG. Influence of phase difference between kinematic and inertial loads on seismic behaviour of pile foundations in layered soils. Https://DoiOrg/101139/Cgj-2019-0547 2020:1–18. https://doi.org/10.1139/CGJ-2019-0547.

[19] Hardin BO, Drnevich VP. Shear Modulus and Damping in Soils: Measurement and Parameter Effects. ASCE J Soil Mech Found Div 1972;98:603–24. https://doi.org/10.1016/0022-4898(73)90212-7.

[20] Viggiani G, Atkinson JH. Stiffness of fine-grained soil at very small strains. Geotechnique 1995;45:249–65. https://doi.org/10.1680/geot.1995.45.2.249.

[21] Oztoprak S, Bolton MD. Stiffness of sands through a laboratory test database. Geotechnique 2013;63:54–70. https://doi.org/10.1680/GEOT.10.P.078.

[22] API. RP 2GEO: Geotechnical and foundation design considerations. Washington, DC, USA: API: 2014.

[23] Matlock H. Correlation for Design of Laterally Loaded Piles in Soft Clay. Offshore Technol. Conf., Houston, Texas: OTC; 1970. https://doi.org/10.4043/1204-MS.

[24] Sullivan WR, Reese LC, Fenske CW. Unified method for analysis of laterally loaded piles in clay. Electron. Ind., London. London: Institution of Civil Engineers; 1980, p. 135–46.

[25] Taciroglu E, Rha C, Wallace JW. A robust Macroelement for Soil-Pile Interaction under Cyclic Loads. J Geotech Geoenvironmental Eng 2006;132:1304–14. https://doi.org/10.1061/(ASCE)1090-0241(2006)132.

[26] O'Neill, MW and Murchison JM. An evaluation of py relationships in sands. A report to the American Petroleum Institute (GT-DF02-83). Houston, Texas: 1983.

[27] Georgiadis M. test Development of P-Y curves for layered soils. Geotech. Pract. Offshore Eng., New York: American Society of Civil Engineers; 1983, p. 536–45. https://doi.org/10.1016/0148-9062(85)92248-X.

[28] Rollins KM, Lane JD, Gerber TM. Measured and Computed Lateral Response of a Pile Group in Sand. J Geotech Geoenvironmental Eng 2005;131:103–14. https://doi.org/10.1061/(asce)1090-0241(2005)131:1(103).

[29] Brown DA, Morrison C, Reese LC. Lateral load behavior of pile group in sand. J Geotech Eng 1988;114:1261–76. https://doi.org/10.1061/(ASCE)0733-9410(1988)114:11(1261).

[30] Fayyazi MS, Taiebat M, Finn WDL. Group reduction factors for analysis of laterally loaded pile groups. Can Geotech J 2014;51:758–69. https://doi.org/10.1139/cgj-2013-0202.

[31] Brown DA, Reese LC, O'Neill MW. Cyclic Lateral Loading of a Large-Scale Pile Group. J Geotech Eng 1987;113:1326–43. https://doi.org/10.1061/(ASCE)0733-9410(1987)113:11(1326).

[32] Rollins KM, Peterson KT, Weaver TJ. Lateral Load Behavior of Full-Scale Pile Group in Clay. J Geotech Geoenvironmental Eng 1998;124:468–78. https://doi.org/10.1061/(asce)1090-0241(1998)124:6(468).

[33] Snyder JL. Full-Scale Lateral-Load Tests of a 3x5 Pile Group in Soft Clays and Silts. (Masters Thesis) Brigham Young University, 2004.

[34] Rollins KM, Olsen R, Egbert J, Olsen K, Jensen D, Garrett B. Response, Analysis, and Design of Pile Groups Subjected to Static & Dynamic Lateral Loads (Report No. UT-03.03). 2003.

[35] Ruesta PF, Townsend FC. Evaluation of Laterally Loaded Pile Group at Roosevelt Bridge. J Geotech Geoenvironmental Eng 1997;123:1153–61. https://doi.org/10.1061/(asce)1090-0241(1997)123:12(1153).

[36] Mostafa YE, Naggar MH El. Dynamic analysis of laterally loaded pile groups in sand and clay. Can Geotech J 2002;39:1358–83. https://doi.org/10.1139/t02-102.

[37] Garala TK, Madabhushi SPG. Role of Pile Spacing on Dynamic Behavior of Pile Groups in Layered Soils. J Geotech Geoenvironmental Eng 2021;147:04021005. https://doi.org/10.1061/(ASCE)GT.1943-5606.0002483.

[38] Fan K, Gazetas G, Kaynia A, Kausel E, Ahmad S. Kinematic seismic response of single piles and pile groups. J Geotech Eng 1991;117:1860–79. https://doi.org/10.1061/(ASCE)0733-9410(1991)117:12(1860).

[39] Margason E, Halloway D. Pile bending during earthquakes. Proc. sixth world Conf. Earthq. Eng., 1977, p. 1690–6.

[40] Di Laora R, Mylonakis G, Mandolini A. Pile-head kinematic bending in layered soil. Earthq Eng Struct Dyn 2013;42:319–37. https://doi.org/10.1002/EQE.2201.

[41] Sanctis L de, Maiorano RMS, Aversa S. A method for assessing kinematic bending moments at the pile head. Earthq Eng Struct Dyn 2010;39:1133–54. https://doi.org/10.1002/EQE.996.

[42] Dobry R, O'Rourke MJ. Discussion of 'Seismic response of end-bearing piles. J Geotech Eng 1983;109:778–781.

[43] Nikolaou A, Mylonakis G, Gazetas G. Kinematic Bending Moments in Seismically Stressed Piles (Report no. NCEER-95-0022). 1995.

[44] Mylonakis G. Simplified Model for Seismic Pile Bending at Soil Layer Interfaces. Soils Found 2001;41:47–58. https://doi.org/10.3208/SANDF.41.4_47.

[45] Di Laora R, Mandolini A, Mylonakis G. Insight on kinematic bending of flexible piles in layered soil. Soil Dyn Earthq Eng 2012;43:309–22. https://doi.org/10.1016/J.SOILDYN.2012.06.020.

[46] Di Laora R, Rovithis E. Kinematic Bending of Fixed-Head Piles in Nonhomogeneous Soil. J Geotech Geoenvironmental Eng 2015;141:04014126. https://doi.org/10.1061/(ASCE)GT.1943-5606.0001270.

[47] Adachi N, Suzuki Y, Miura K. Correlation between inertial force and subgrade reaction of pile in liquefied soil. 13 th World Conf. Earthq. Eng., Vancouver, B.C., Canada: 2004, p. 332.

[48] Tokimatsu K, Suzuki H, Sato M. Effects of inertial and kinematic interaction on seismic behavior of pile with embedded foundation. Soil Dyn Earthq Eng 2005;25:753–62. https://doi.org/10.1016/j.soildyn.2004.11.018.

[49] Georgiadis M. Development of P-Y curves for layered soils. Int J Rock Mech Min Sci Geomech Abstr 1985;22:158. https://doi.org/10.1016/0148-9062(85)92248-X.

[50] Yang Z, Jeremić B. Study of Soil Layering Effects on Lateral Loading Behavior of Piles. J Geotech Geoenvironmental Eng 2005;131:762–70. https://doi.org/10.1061/(ASCE)1090-0241(2005)131:6(762).

[51] Burd HJ, Abadie CN, Byrne BW, Houlsby GT, Martin CM, McAdam RA, et al. Application of the PISA design model to monopiles embedded in layered soils. Géotechnique 2020;70:1067–82. https://doi.org/10.1680/jgeot.20.PISA.009.

[52] Suryasentana SK, Lehane BM. Verification of numerically derived CPT based p-y curves for piles in sand. 3rd Int. Symp. Cone Penetration Test., Las Vegas, Nevada, United States: 2014, p. 1013–20.

[53] Suryasentana SK, Lehane BM. Updated CPT-based p – y formulation for laterally loaded piles in cohesionless soil under static loading. Géotechnique 2016;66:445–53. https://doi.org/10.1680/jgeot.14.P.156.

[54] Ariannia SS. Determination of p-y Curves by Direct Use of Cone Penetration Test (CPT) Data. (Doctoral Thesis) University of California, 2017.